JVST A
Journal of Vacuum Science & Technology A

Van der Waals epitaxy and remote epitaxy of $LiNbO_3$ thin films by pulsed laser deposition

EP

Cite as: J. Vac. Sci. Technol. A **39**, 040405 (2021); https://doi.org/10.1116/6.0001109
Submitted: 01 May 2021 . Accepted: 08 June 2021 . Published Online: 25 June 2021

Ru Jia, Hyun S. Kum, Xin Sun, Yuwei Guo, Baiwei Wang, Peijiao Fang, Jie Jiang, Daniel Gall, Toh-Ming Lu, Morris Washington, Jeehwan Kim, and Jian Shi

JVST A
Journal of Vacuum Science & Technology A

LETTER

avs.scitation.org/journal/jva

Van der Waals epitaxy and remote epitaxy of $LiNbO_3$ thin films by pulsed laser deposition

Cite as: J. Vac. Sci. Technol. A **39**, 040405 (2021); doi: 10.1116/6.0001109
Submitted: 1 May 2021 · Accepted: 8 June 2021 ·
Published Online: 25 June 2021

View Online Export Citation CrossMark

Ru Jia,[1] Hyun S. Kum,[2] Xin Sun,[3] Yuwei Guo,[1] Baiwei Wang,[1] Peijiao Fang,[1] Jie Jiang,[1] Daniel Gall,[1] Toh-Ming Lu,[3] Morris Washington,[3] Jeehwan Kim,[2] and Jian Shi[1,a)]

AFFILIATIONS

[1]Department of Materials Science and Engineering, Rensselaer Polytechnic Institute, Troy, New York 12180
[2]Department of Mechanical Engineering, Massachusetts Institute of Technology, Cambridge, Massachusetts 02138
[3]Center for Materials, Devices and Integrated Systems and Department of Physics, Applied Physics and Astronomy, Rensselaer Polytechnic Institute, Troy, New York 12180

[a)]**Electronic mail:** shij4@rpi.edu

ABSTRACT

Nonlinear oxides such as $LiNbO_3$ have found many applications in both conventional electro-optics and quantum optics. In this work, we demonstrate the van der Waals and remote epitaxy of $LiNbO_3$ films on muscovite mica and graphene-buffered sapphire, respectively, by pulsed laser deposition. Structural analysis shows that the epitaxial relation in van der Waals epitaxy is $LiNbO_3$ (0001) || mica (001) and $LiNbO_3$ $[01\bar{1}0]$ || mica [010] with $LiNbO_3$ $[10\bar{1}0]$ || mica [010], a 60°-rotated twin structure. The relation in remote epitaxy is $LiNbO_3$ (0001) || sapphire (0001) and $LiNbO_3$ $[01\bar{1}0]$ || sapphire $[01\bar{1}0]$ with twin structure $LiNbO_3$ $[\bar{1}010]$ || sapphire $[01\bar{1}0]$. Furthermore, in remote epitaxy, Raman scattering analysis confirms the existence of graphene after deposition. Finally, we find that the oxygen partial pressure influences the presence of impurity phases significantly. The successful demonstration of van der Waals and remote epitaxy promises the feasibility of developing thin film $LiNbO_3$ on demanded substrates toward scalable electro-optics.

I. INTRODUCTION

Nonlinear optical phenomena such as the Kerr effect, frequency mixing processes, and cross-phase modulation result from nonlinear interaction of the electromagnetic field with noncentrosymmetric crystals. Major applications of nonlinear optical phenomena include ultrashort pulsed lasers, sensors, laser amplifiers, and digital optical information processing, among many others.[1] A recently proposed application lies in the field of quantum computing, which includes spontaneous parametric downconversion that is used to produce entangled photons.[2]

$LiNbO_3$ (R3c, $a = b = 5.212$ Å, $c = 14.356$ Å, $\alpha = \beta = 90°$, and $\gamma = 120°$) is one of the most widely used materials for nonlinear optics.[3] Apart from having a wide transmission window (0.35–5 μm), high refractive indices ($n_o = 2.286$, $n_e = 2.203$ at 632.8 nm), and high second-order susceptibilities ($d_{31} = -4.88$ pm/V, $d_{33} = 34.0$ pm/V), it is also ferroelectric in nature, making the reconfigurability of its nonlinear property by an electric field possible.[4,5] For applications in photonic integrated circuits, $LiNbO_3$ in thin film form as opposed to the bulk form is necessary. Thin films can be applied to reduce device dimensions and the operating voltage, making it easier to modulate electrical and optical properties.

Over the past few decades, several methods have been used to grow $LiNbO_3$ thin films, including pulsed laser deposition (PLD),[6] RF sputtering,[7] metal-organic chemical vapor deposition,[8] as well as solgel process.[9] Highly demanded epitaxial growth of $LiNbO_3$ has been reported on many substrates, such as ZnO/Si,[10] MgO,[11,12] sapphire,[6,13] and $LiTaO_3$.[14,15] In the pursuit of high-quality and transferable thin films, van der Waals epitaxy[16,17] (in which film-substrate interaction is believed to be van der Waals or quasi van der Waals based) and remote epitaxy[18,19] (in which film-substrate interaction is remotely controlled by a buffer layer of 2D materials such as graphene) have been regarded as promising solutions. In the past few years, we have demonstrated the van der Waals and remote epitaxy of several halide perovskites, chalcogenides, and complex oxides.[18,20–27] In some of these works, we have found that remote and van der Waals epitaxial films could be mechanically exfoliated and transferred onto arbitrary substrates.[18]

Here, we report the growth of epitaxial $LiNbO_3$ thin films based on van der Waals epitaxy as well as remote epitaxy. For van der Waals epitaxy, muscovite mica (C2/c, a = 5.199 Å, b = 9.027 Å, c = 20.106 Å, $\alpha = \gamma = 90°$, and $\beta = 95.78°$) is chosen as the substrate. Prior to growth, the heterostructure of $LiNbO_3$/mica is proposed in Figs. 1(a)–1(c). The pseudohexagonal lattice structure of mica with a ≈ 5.18 Å matches well with that of $LiNbO_3$ (less than 0.5% mismatch), as shown in Fig. 1(c). For remote epitaxy, graphene covered sapphire (sapphire: $R\bar{3}c$, a = b = 4.760 Å, c = 12.993 Å, $\alpha = \beta = 90°$, and $\gamma = 120°$) is chosen as the substrate. Figures 1(d)–1(f) presents our proposed heterostructure of $LiNbO_3$/graphene/sapphire. As shown in Fig. 1(f), the lattice mismatch of lattice parameter a between sapphire and $LiNbO_3$ is about 8.7%, which is large but still feasible for the execution of epitaxy.

II. EXPERIMENT

All thin film growth was executed by a home-built PLD system (KrF excimer laser, λ = 248 nm) using a 2 in.-diameter commercial $LiNbO_3$ target. The laser power density during deposition was about 7.5 J/cm^2. The target-to-substrate distance was set as 5 cm. $LiNbO_3$ thin films were grown on freshly cleaved muscovite mica at 550 °C with the oxygen pressure ranging from 300 to 600 mTorr. $LiNbO_3$ was deposited on graphene-buffered sapphire

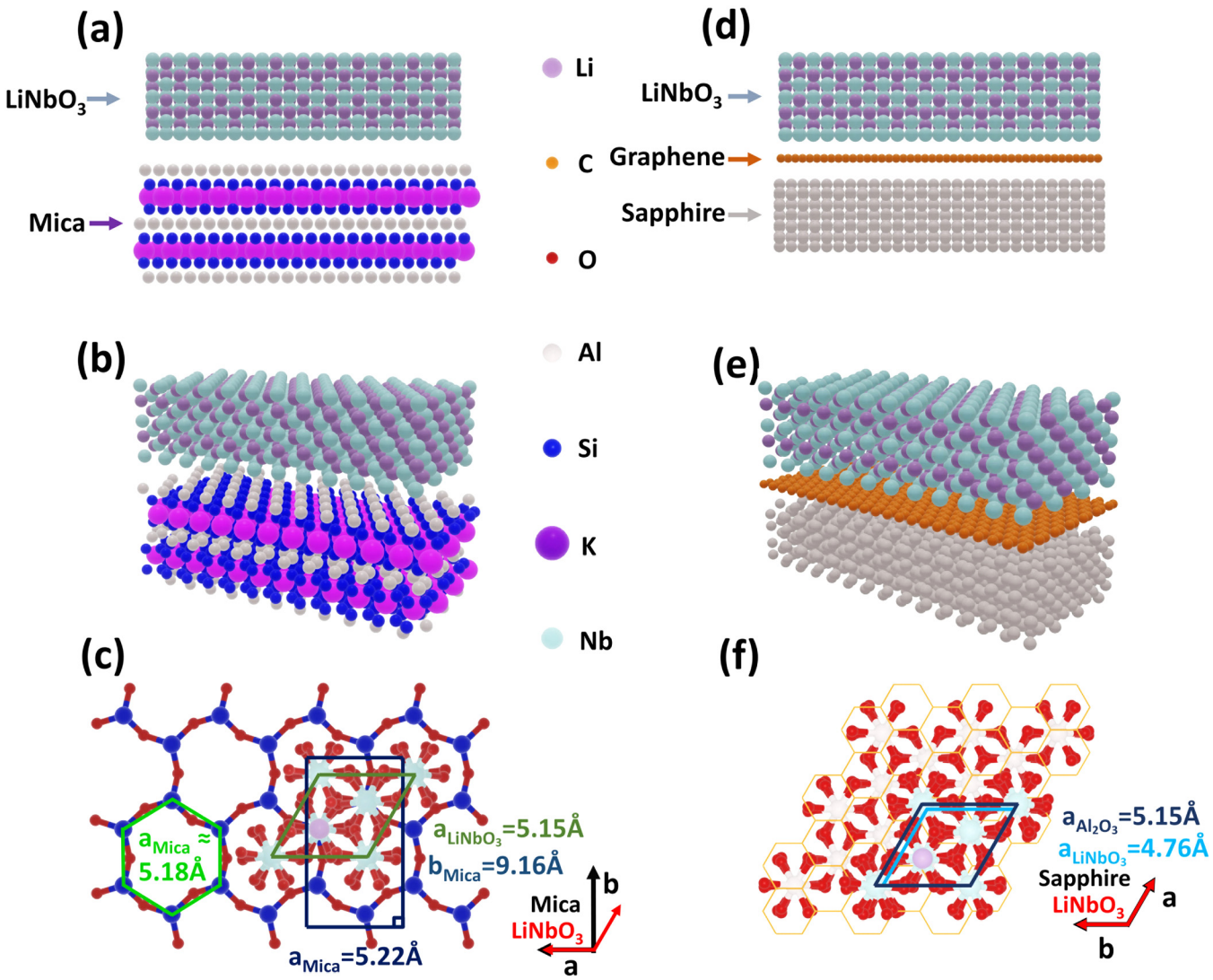

FIG. 1. Schematics of the proposed heterostructure. (a)–(c) Heterostructure of $LiNbO_3$ film grown on mica (001). (d)–(f) Heterostructure of $LiNbO_3$ film grown on graphene-buffered sapphire (0001). (a) and (d) Front view; (b) and (e) bird view; and (c) and (f) proposed lattice models.

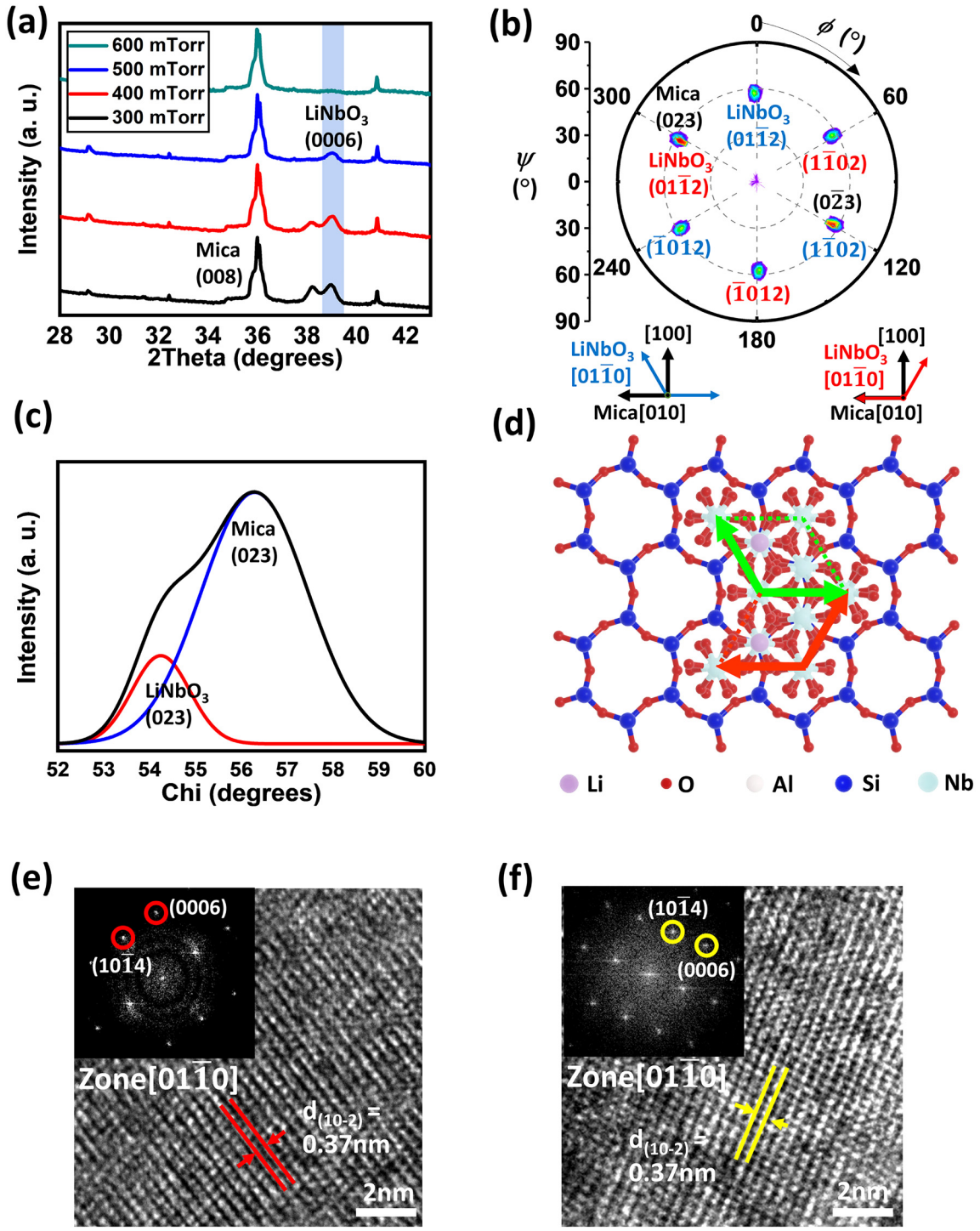

FIG. 2. Van der Waals epitaxial $LiNbO_3$ films on mica (001). (a) XRD ω-2θ spectra of films grown at 550 °C with the oxygen pressure ranging from 300 to 600 mTorr; (b) pole figure of epitaxial $LiNbO_3$ (01$\bar{1}$2) planes. The thick and thin crystal axes drawn at the bottom right are for mica and $LiNbO_3$, respectively; (c) χ scan of the overlapping peak from $LiNbO_3$ (01$\bar{1}$2) and mica (023) plane; (e) and (f) HRTEM images for different orientations of $LiNbO_3$ grains along with their FFT in the inset; and (d) atomic model of the $LiNbO_3$/mica heterostructure showing their epitaxial relations.

(0001) at an optimized condition of 550 °C and 500 mTorr oxygen pressure. All the films were postannealed at 550 °C in 760 Torr oxygen pressure.

Monolayer graphene, synthesized on Cu foils by chemical vapor deposition, was purchased from Graphene Laboratories Inc. (Calverton, New York, USA). For graphene transfer, poly(methyl methacrylate) (PMMA) was first spin-coated onto the graphene/Cu foil as a support. The rear side of the Cu foil was then treated in an O_2 plasma etcher to remove unwanted graphene. The Cu foils were etched in an ammonium persulfate aqueous solution (60 g/l).

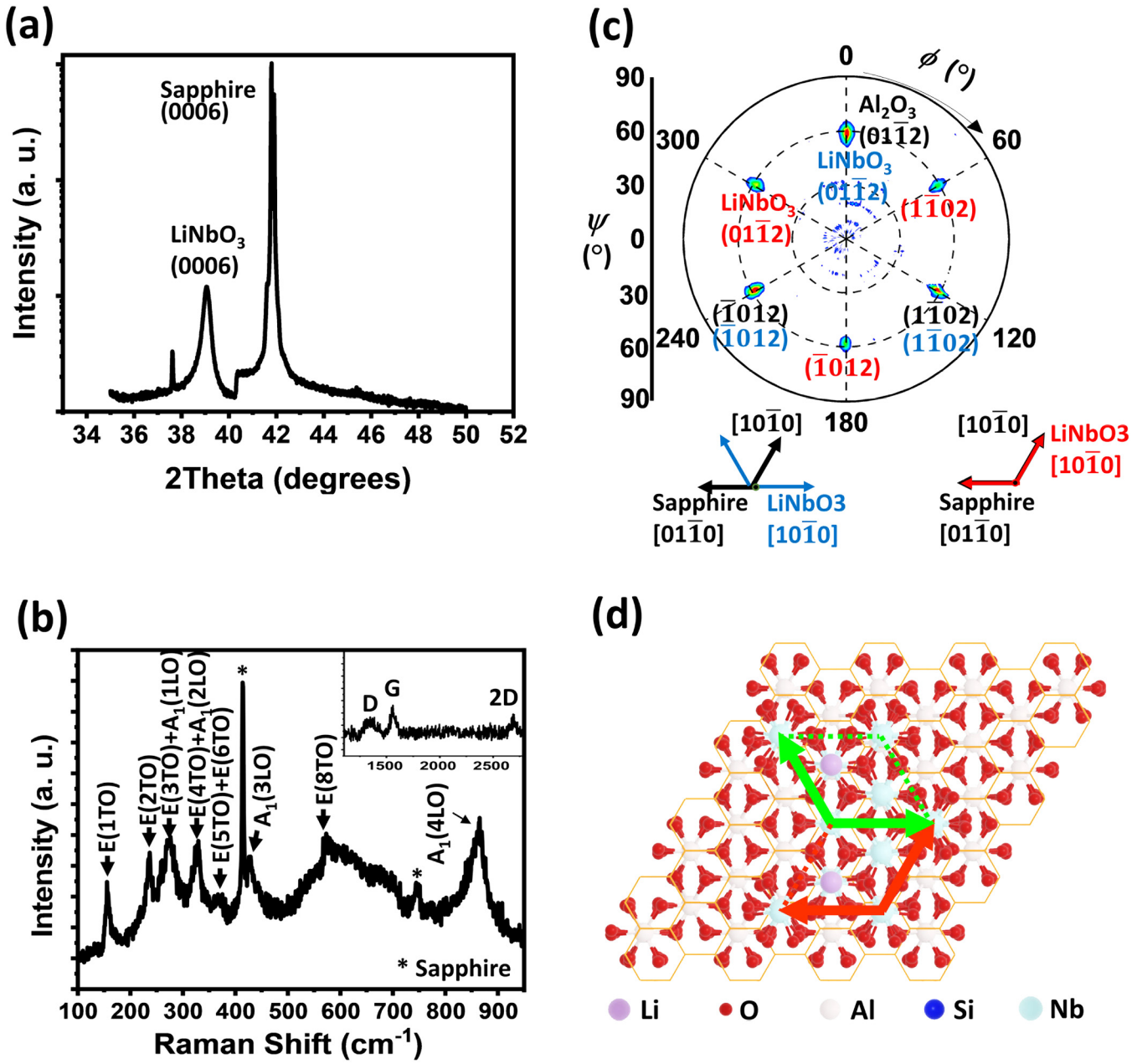

FIG. 3. Remote epitaxial $LiNbO_3$ films on graphene/sapphire, deposited at 550 °C in 500 mTorr oxygen. (a) XRD ω-2θ spectrum; (b) Raman spectrum, the inset of which shows the peak from the graphene after $LiNbO_3$ deposition; (c) pole figure of $LiNbO_3$ (01$\bar{1}$2) planes; and (d) atomic model of the $LiNbO_3$/graphene/sapphire heterostructure showing their epitaxial relations.

The PMMA/graphene assembly was rinsed in water several times and picked up by the sapphire (0001) substrate. The PMMA/graphene/sapphire (0001) stack was dried in air and followed by the dissolution of PMMA in acetone. After these procedures, the graphene/sapphire substrate is ready for PLD growth.

The structure of the grown $LiNbO_3$ films was characterized by x-ray diffraction (XRD) with a Cu K_α radiation (Panalytical X'pert PRO MPD system). X-ray pole figures were obtained using point focus optics with a polycapillary x-ray lens to study the in-plane orientation. High-resolution transmission electron microscopy (HRTEM) images of the $LiNbO_3$ on mica were acquired by an FEI F20 TEM at 200 kV. A Helios G4 UX focused ion beam system was used to cut a cross section of the thin film. Raman spectra (WITec Alpha 300R Confocal Raman imaging system) were collected to confirm the composition of $LiNbO_3$ on the graphene-buffered sapphire (0001) and check the integrity of the graphene buffer layer after film growth.

III. RESULTS AND DISCUSSION

A. $LiNbO_3$ thin films grown on muscovite mica

Figure 2(a) shows the XRD pattern of $LiNbO_3$ thin films grown on mica. The peak at 39.0° denotes the $LiNbO_3$ (0006) plane. The peak at 36.0° is recognized as muscovite mica (008)[28] and peaks at 29.1°, 32.4°, and 40.8° are all from the cleaved mica substrate (see the supplementary material[35] for detailed indices). A series of oxygen partial pressures were applied during growth to minimize the Li-deficient phase, $LiNb_3O_8$. Only for films grown in 500 mTorr oxygen pressure, no peaks other than the $LiNbO_3$ (0006) peak are observed. There is an additional peak at 38.1° for films grown in relatively low oxygen pressure (300 and 400 mTorr), which corresponds to the $LiNb_3O_8$ ($\bar{6}02$) peak.[29] This observation can be explained by the suppression of oxidation of Li atoms in the oxygen-rich environment.[13] When the oxygen pressure is increased to 600 mTorr, the $LiNbO_3$ peak disappears since collisions between the ablated species and oxygen atoms increase and crystallization may be hindered by the reduced kinetic energy of the ablated atoms.[30,31]

Figure 2(b) shows the x-ray pole figure used to determine the in-plane orientation of the $LiNbO_3$ thin film. Two sets of $(01\bar{1}2)$ planes are seen in the pole figure, which indicates a 60°-rotated twin structure. The two reflections with an abnormal intensity were further studied along their χ direction. The χ scan result at $2\theta = 23.7°$ is shown in Fig. 2(c). It can be seen that the (023) plane of mica and the $(01\bar{1}2)$ reflection of $LiNbO_3$ overlap, which reveals the in-plane epitaxial relation as mica [010] || $LiNbO_3$ $[01\bar{1}0]$ and mica [010] || $LiNbO_3$ $[10\bar{1}0]$. The cross-sectional HRTEM images of the $LiNbO_3$ thin film with a zone axis of $[01\bar{1}0]$ in Figs. 2(e) and 2(f) also confirm the 60°-rotated twin structure. From the inset fast Fourier transform (FFT) pattern, the interplanar spacing of $(10\bar{1}\bar{2})$ planes is 0.37 nm, which corresponds well with that of bulk $LiNbO_3$. The twin structure of the atomic model is shown in Fig. 2(d).

B. $LiNbO_3$ thin films grown on graphene-buffered sapphire (0001)

Figure 3(a) shows the XRD pattern of $LiNbO_3$ thin films grown at 500 °C and 500 mTorr oxygen pressure on a graphene-buffered sapphire (0001) substrate. A clear $LiNbO_3$ (0006) peak can be seen. The peak at 41.7° is attributed to the sapphire (0006) peak. The peak at 37.5° is also from the substrate. The Raman spectrum in Fig. 3(b) shows the $9E(TO) + 4A_1(LO)$ modes of $LiNbO_3$,[32,33] except for the E(7TO) at ~430 cm^{-1} and E(9TO) at ~660 cm^{-1} modes, which have intensities too small to be identified. The inset of Fig. 3(b) shows the Raman spectrum ranging from 1100 to 2800 cm^{-1} of the same measurement. The G (~1580 cm^{-1}) and 2D (~2680 cm^{-1}) peaks of graphene can be clearly identified in the spectrum indicating the existence of graphene after growth. The existence of a small D (~1350 cm^{-1}) peak indicates that the graphene buffer layer has been partially damaged by the oxygen atmosphere and the high-energy plasma at high temperatures.[34]

The in-plane symmetry of the grown film was determined from the x-ray pole figure in Fig. 3(c). The two sets of $(01\bar{1}2)$ planes indicate a twin structure in $LiNbO_3$ as also seen in the $LiNbO_3$ film grown on mica. Thus, there are two sets of in-plane symmetry relations, sapphire $[10\bar{1}0]$ || $LiNbO_3$ $[10\bar{1}0]$ and sapphire $[10\bar{1}0]$ || $LiNbO_3$ $[11\bar{2}0]$ in the 60°-rotated twin structure, as shown in Fig. 3(d).

IV. SUMMARY AND CONCLUSIONS

In summary, we demonstrated the growth of epitaxial $LiNbO_3$ film via van der Waals and remote epitaxy by pulsed laser deposition. Structural analysis has revealed the epitaxy relations and identified the presence of twin structures of $LiNbO_3$ films in both $LiNbO_3$/mica and $LiNbO_3$/graphene/sapphire systems. In remote epitaxy, Raman spectroscopy has confirmed the existence of graphene after deposition suggesting the active role of graphene during the deposition process. The demonstration of the feasibility of van der Waals and remote epitaxy of $LiNbO_3$ suggests a promising processing route toward the development of free-standing $LiNbO_3$ films in the near future.

ACKNOWLEDGMENTS

This work was supported by the U.S. Air Force Office of Scientific Research under Grant No. FA9550-18-1-0116 (R.J. and J.S.) and the NYSTAR Focus Center at Rensselaer Polytechnic Institute (RPI) with Contract No. C150117 (X.S., T.-M.L, M.W., and J.S.). The authors declare no competing interests. This work is also supported by U.S. National Science Foundation under Award No. of 1712752 (D.G.). This paper is also supported by the U.S. National Science Foundation [Platform for the Accelerated Realization, Analysis, and Discovery of Interface Materials (PARADIM)] under Cooperative Agreement No. DMR-1539918 and made use of the Cornell Center for Materials Research (CCMR) Shared Facilities, which are supported through the NSF MRSEC Program (No. DMR-1719875).

DATA AVAILABILITY

The data that support the findings of this study are available from the corresponding author upon reasonable request.

REFERENCES

[1] C. Li, *Nonlinear Optics: Principles and Applications* (Springer Singapore, Singapore, 2017).

[2]H. Jin *et al.*, Phys. Rev. Lett. **113**, 103601 (2014).
[3]C. Wang, M. Zhang, X. Chen, M. Bertrand, A. Shams-Ansari, S. Chandrasekhar, P. Winzer, and M. Lončar, Nature **562**, 101 (2018).
[4]L. Arizmendi, Phys. Status Solidi A **201**, 253 (2004).
[5]M. J. Weber, *Handbook of Optical Materials* (CRC, Raton, 2002).
[6]S. H. Lee, T. K. Song, T. W. Noh, and J. H. Lee, Appl. Phys. Lett. **67**, 43 (1995).
[7]G. M. Hewig, K. Jain, F. O. Sequeda, R. Tom, and P.-W. Wang, Thin Solid Films **88**, 67 (1982).
[8]Z. Lu, R. Hiskes, S. A. DiCarolis, R. K. Route, R. S. Feigelson, F. Leplingard, and J. E. Fouquet, J. Mater. Res. **9**, 2258 (1994).
[9]K. Nashimoto and M. J. Cima, Mater. Lett. **10**, 348 (1991).
[10]S. Shandilya, M. Tomar, and V. Gupta, J. Appl. Phys. **111**, 102803 (2012).
[11]D. K. Fork, F. Armani-Leplingard, J. J. Kingston, and G. B. Anderson, Mater. Res. Soc. Symp. Proc. **361**, 155 (1995).
[12]K. Nunomura, A. Ishitani, T. Matsubara, and I. Hayashi, J. Cryst. Growth **45**, 355 (1978).
[13]Y. Kakehi, A. Okamoto, Y. Sakurai, Y. Nishikawa, T. Yotsuya, and S. Ogawa, Appl. Surf. Sci. **169–170**, 560 (2001).
[14]T. Fukuda and H. Hirano, Appl. Phys. Lett. **28**, 575 (1976).
[15]S. Kondo, S. Miyazawa, S. Fushimi, and K. Sugii, Appl. Phys. Lett. **26**, 489 (1975).
[16]A. Koma, K. Sunouchi, and T. Miyajima, Microelectron. Eng. **2**, 129 (1984).
[17]Y. Bitla and Y.-H. Chu, Nanoscale **12**, 18523 (2020).
[18]Y. Kim *et al.*, Nature **544**, 340 (2017).
[19]J. Shim *et al.*, Carbon **133**, 78 (2018).
[20]Y. Wang, Y. Shi, G. Xin, J. Lian, and J. Shi, Cryst. Growth Des. **15**, 4741 (2015).
[21]X. Sun, Z. Lu, W. Xie, Y. Wang, J. Shi, S. Zhang, M. A. Washington, and T.-M. Lu, Appl. Phys. Lett. **110**, 153104 (2017).
[22]Y. Wang, Z. Chen, F. Deschler, X. Sun, T.-M. Lu, E. A. Wertz, J.-M. Hu, and J. Shi, ACS Nano **11**, 3355 (2017).
[23]D. Mohanty *et al.*, Phys. Rev. Mater. **2**, 113402 (2018).
[24]J. Jiang *et al.*, Nat. Commun. **10**, 4145 (2019).
[25]Y. Guo *et al.*, Nano Lett. **20**, 33 (2020).
[26]H. S. Kum *et al.*, Nature **578**, 75 (2020).
[27]S. Pendse *et al.*, J. Cryst. Growth **543**, 125699 (2020).
[28]Y. Wang *et al.*, Adv. Mater. **28**, 8975 (2016).
[29]A. Bartasyte, V. Plausinaitiene, A. Abrutis, S. Stanionyte, S. Margueron, P. Boulet, T. Kobata, Y. Uesu, and J. Gleize, J. Phys.: Condens. Matter **25**, 205901 (2013).
[30]S. H. Lee, T. W. Noh, and J. H. Lee, Appl. Phys. Lett. **68**, 472 (1996).
[31]X. Wang, Y. Liang, S. Tian, W. Man, and J. Jia, J. Cryst. Growth **375**, 73 (2013).
[32]M. A. Fakhri, Evan T. Salim, R. A. Ismail, A. W. Abdulwahhab, Z. T. Salim, M. A. Munshid, and U. Hashim, Indian J. Eng. Mater. Sci. **15**, 355 (2008).
[33]S. Margueron, A. Bartasyte, A. M. Glazer, E. Simon, J. Hlinka, I. Gregora, and J. Gleize, J. Appl. Phys. **111**, 104105 (2012).
[34]M. Currie, J. D. Caldwell, F. J. Bezares, J. Robinson, T. Anderson, H. Chun, and M. Tadjer, Appl. Phys. Lett. **99**, 211909 (2011).
[35]See supplementary material at https://www.scitation.org/doi/suppl/10.1116/6.0001109 for XRD of the bare mica substrate.